Efficient Targeted Energy Transfer With Parallel Nonlinear Energy Sinks: Theory and Experiments

Bastien Vaurigaud, Alireza Ture Savadkoohi, Claude-Henri Lamarque

Efficient Targeted Energy Transfer With Parallel Nonlinear Energy Sinks: Theory and Experiments

Bastien Vaurigaud, Alireza Ture Savadkoohi, Claude-Henri Lamarque

Université de Lyon ENTPE, DGCB FRE CNRS 3237, rue Maurice Audin, 69518 Vaulx-en-Velin Cedex, France

In this paper the targeted energy transfer (TET) phenomenon between a linear multi-DOF master structure and several slave parallel nonlinear energy sink (NES) devices during a 1:1 resonance capture is investigated. An analytical method is proposed for tuning optimal NES parameters, which leads to efficient TETs. Then, the procedure is intentionally narrowed for a 4DOF master structure with two parallel NESs at the last DOF in order to grasp optimum NES parameters of a prototype structure that is built and tested at the Civil Engineering and Building Department Laboratory of the ENTPE. The aim is to control the first mode of the compound nonlinear prototype system by demon-strating the efficiency of designed parallel NESs by the suggested method.

1 Introduction

By endowing the nonlinear innate of special absorber systems, namely, NES devices, safe and appropriate control of mechanical and structural systems for wide frequency bands is possible. A good summary of theoretical background of these systems can be found in Refs. [1,2]. Outstanding abilities of these devices in controlling systems against vibratory forces are also verified experimentally; from them we can mention to experimental studies of McFarland et al. [3,4], Kerschen et al. [5,6], Gourdon et al. [7,8], Manevitch et al. [9], and Lee et al. [10–12]. All of the above mentioned theoretical and experimental studies were carried out on structures with single NES devices. In this paper we will present analytical methods for designing optimal parallel NES devices that are accompanied by couple of experimental tests, which are carried out at the Civil Engineering and Building Department (DGCB) Laboratory of the ENTPE, France. The organization of the paper is given as follows.

The academic representation of the system and necessary condition for an optimized and efficient design of NESs are reported in Sec. 2. The system under harmonic solicitation is investigated in Sec. 3. Multiple solutions, linear stability analysis, and some numerical examples are reported at the same section. Section 4 illustrates some experimental results on a 4DOF prototype structure with two parallel NESs at the last floor. Finally conclusion remarks are gathered in Sec. 5.

2 Mathematical Model of the System

Figure 1 illustrates a p DOF linear system where M_n, C_n, K_n, and X_n are mass, damping, stiffness, and displacement of each nth DOF, $n=1,2,\ldots,p$, respectively. $F=[F_1\cdots F_n\cdots F_p]^T$ is the applied external forcing vector to the system. Each DOF n is coupled to n_n parallel cubic NES: $\mu_{n,j}$, $c_{n,j}$, $k_{n,j}$, and $x_{n,j}$, $j=1,2,\ldots n_n$ are mass, damping, stiffness, and the displacement of the attached jth NES to the same DOF. So, the whole compound system has $(n_1+n_2+\cdots+n_p)$ NES. By shifting from physical domain to the modal domain by $\mathbf{X}=\phi\mathbf{q}$ (ϕ and $\mathbf{q}$ are mode shape matrix and modal coordinate vector), the mathematical representation of the system during its first mode (the one which is intended to be controlled) reads as

$$\begin{cases} M_1^*\ddot{q}_1 + C_1^*\dot{q}_1 + K_1^*q_1 + \sum_{l=1}^{p}\sum_{j=1}^{n_l}\phi_{l,1}\mu_{l,j}\ddot{x}_{l,j} = \sum_{l=1}^{p}\phi_{l,1}F_l(t) \\ \forall n=1\cdots p, \quad \forall j=1\ldots n_n \\ \mu_{n,j}\ddot{x}_{n,j} + c_{n,j}(\dot{x}_{n,j}-\phi_{n,1}\dot{q}_1) + k_{n,j}(x_{n,j}-\phi_{n,1}q_1)^3 = 0 \end{cases} \tag{1}$$

where M_1^*, C_1^*, and K_1^* are first mode modal mass, damping, and stiffness of the linear system while $\phi_{n,1}$ is the first mode modal shape of the linear system at DOF n. First of all we consider the system under impulse loading ($F_l(t)=0$) with the following initial conditions:

$$\begin{cases} q_1(0)=0, \quad \dot{q}_1(0)\neq 0 \\ x_{n,j}(0)=\dot{x}_{n,j}(0)=0, \quad \forall n=1\cdots p, \quad \forall j=1\cdots n_n \end{cases} \tag{2}$$

We are interested to investigate the system under 1:1 resonance. Let us assume $\mu_{n,j}/M_1^*=\varepsilon\alpha_{n,j}$, $\Sigma_{n=1}^{p}\Sigma_{j=1}^{n_l}\alpha_{n,j}=1$, $c_{n,j}/M_1^*=\varepsilon\alpha_{n,j}\lambda_{n,j}$, $k_{n,j}/M_1^*=\varepsilon\alpha_{n,j}\Omega_{n,j}\omega_0^{*4}$, $C_1^*/M_1^*=\varepsilon\lambda^*$, and $K_1^*/M_1^*=\omega_0^{*2}$. Moreover, we shift the system to the new coordinates as follows:

$$\begin{cases} u = q_1 + \varepsilon\sum_{l=1}^{p}\sum_{j=1}^{n_l}\phi_{l,1}\alpha_{l,j}x_{l,j} \\ v_{n,j} = x_{n,j} - \phi_{n,1}q_1, \quad \forall n=1\cdots p, \quad \forall j=1\cdots n_n \end{cases} \tag{3}$$

The final form of Eq. (2) under impulse loading is given as follows:

$$(\ddot{u}+\omega_0^{*2}u) + \varepsilon\left[\lambda^*\dot{u} + \omega_0^{*2}\sum_{l=1}^{p}\sum_{j=1}^{n_l}\alpha_{n,j}\phi_{n,j}v_{n,j}\right] - \varepsilon\left[\omega_0^{*2}\sum_{l=1}^{p}\sum_{j=1}^{n_l}\alpha_{n,j}\phi_{n,j}^2 u\right] + o(\varepsilon^2) = 0 \tag{4}$$

$$\varepsilon(\ddot{v}_{n,j}+\omega_0^{*2}v_{n,j}) + \varepsilon\phi_{n,j}\omega_0^{*2}u + \varepsilon\lambda_{n,j}\dot{v}_{n,j} + \varepsilon\Omega_{n,j}\omega_0^{*4}v_{n,j}^3 - \varepsilon\omega_0^{*2}v_{n,j} + o(\varepsilon^2) = 0, \quad \forall n=1\cdots p, \quad \forall j=1\cdots n_n \tag{5}$$

Complex variables of Manevitch [13] and multiple scale expansions [14] are introduced in Eqs. (4) and (5) according to the following relations:

$$\varphi_0 e^{i\omega_0^* t} = \dot{u} + i\omega_0^* u$$

$$\varphi_{n,j}e^{i\omega_0^* t} = \dot{v}_{n,j} + i\omega_0^* v_{n,j}, \quad \forall n=1\cdots p, \quad \forall j=1\cdots n_n$$

$$\varphi_0 = \varphi_{00} + \varepsilon\varphi_{01} + \varepsilon^2\varphi_{02} + \cdots \tag{6}$$

[1]Corresponding author.

$$\forall n=1\cdots p,\quad \forall j=1\cdots n_n,\quad \varphi_{n,j}=\varphi_{nj0}+\varepsilon\varphi_{nj1}+\varepsilon^2\varphi_{nj2}+\cdots$$

$$\text{for } l=0,1,2,\ldots,\quad T_l=\varepsilon^l t,\quad \frac{d}{dt}=\frac{\partial}{\partial T_0}+\varepsilon\frac{\partial}{\partial T_1}+\varepsilon^2\frac{\partial}{\partial T_2}+\ldots$$

By progressing until the order ε^1, dropping secular terms, and rewriting complex variables in the polar domain as

$$\begin{cases}\varphi_{00}=R_0(T_1)e^{i\delta_0(T_1)}\\ \Phi_{nj0}=R_{nj}(T_1)e^{i\delta_{n,j}(T_1)},\quad \forall n=1\cdots p,\quad \forall j=1\cdots n_n\end{cases} \tag{7}$$

one can reach the following systems of equations:

$$\begin{cases}\dfrac{1}{\omega_0^*}\dfrac{\partial R_0^2}{\partial T_1}=-\zeta^* R_0^2-\displaystyle\sum_{l=1}^{p}\sum_{j=1}^{n_l}\alpha_{n,j}\zeta_{n,j}R_{nj}^2\\ \phi_{n,j}^2R_0^2=\left[\zeta_{n,j}^2+\left(1-\dfrac{3\Omega_{n,j}}{4}R_{nj}^2\right)^2\right]R_{nj}^2,\quad \forall n=1\cdots p,\quad \forall j=1\cdots n_n\end{cases} \tag{8}$$

where $\zeta^*=\lambda^*/\omega_0^*$ and $\zeta_{n,j}=\lambda_{n,j}/\omega_0^*$. Let us introduce $E_{nj}=\Omega_{n,j}R_{nj}^2$ and $E_0=\Omega_{n,j}R_0^2$, then Eq. (8) reads as

$$\frac{\partial E_0}{\partial T_1}=-\lambda^* E_0-\sum_{l=1}^{p}\sum_{j=1}^{n_l}\alpha_{n,j}\lambda_{n,j}E_{nj} \tag{9}$$

$$\phi_{n,j}^2E_0=\left[\zeta_{n,j}^2+\left(1-\frac{3}{4}E_{nj}\right)^2\right]E_{nj},\quad \forall n=1\ldots p,\quad \forall j=1\ldots n_n \tag{10}$$

where E_0 and E_{nj} are dimensionless variables that depend on initial conditions and the nonlinearity of the system.

$$\begin{cases}E_0=\Omega_{n,j}|\varphi_{00}|^2=\Omega_{n,j}(\dot{u}_0^2+\omega_0^{*2}u_0^2)\\ \forall n=1\cdots p,\quad \forall j=1\cdots n_n\\ E_{nj}=\Omega_{n,j}|\Phi_{nj0}|^2=\Omega_{n,j}(\lim\limits_{T_0\to\infty}[\dot{v}_{nj0}^2+\omega_0^{*2}v_{nj0}^2])\end{cases} \tag{11}$$

2.1 Tuning the NES. The two principles of linear additivity and separated activity of parallel NESs underline that the efficiency of each NES, in the first order approximation, is entirely governed by its own physical parameters, i.e., m_{nj}, c_{nj}, and k_{nj}. This leads us to be able to study the energy activation level for the TET by considering the energy of the master structure, which is donated to each single NES. Figure 2 shows the multiplicity of solution computed from Eq. (10). It has been demonstrated in previous researches [15] that this multiplicity is responsible for the TET. In fact, this bifurcation defines an area where the energy can suddenly jump from high to low levels.

This area of bifurcation can be analytically studied from the derivative of Eq. (10) as

$$\frac{dE_0}{dE_{nj0}}=\frac{1}{\phi_{n,j}^2}\left[\frac{27}{16}E_{nj0}^2-3E_{nj0}+(1+\zeta_{n,j}^2)\right] \tag{12}$$

If $\zeta_{n,j}\in[0,1/\sqrt{3}]$, then we may obtain multiple solutions for Eq. (12). This is a known result in TET. The bifurcation that leads to the energy pumping, due to multiplicity of solutions, only occurs for small values of damping of absorbers [16]. There are two extreme limits in the curve of Fig. 2: E_0^+ and E_0^-, respectively. These coordinates are given by the nullity of derivative of Eq. (12). For the sake of simplicity we define the following functions:

$$\begin{cases}\Delta(\zeta)=9-\dfrac{27}{4}(1+\zeta^2)\\ \gamma^+(\zeta)=\dfrac{24+8\sqrt{\Delta(\zeta)}}{27},\quad \gamma^-(\zeta)=\dfrac{24-8\sqrt{\Delta(\zeta)}}{27}\end{cases} \tag{13}$$

$$\begin{cases}(E_{nj0}^-;E_0^+)=\left[\gamma^-(\zeta_{n,j});\dfrac{1}{\phi_{n,j}^2}\left(\zeta_{n,j}^2+\left(1-\dfrac{3}{4}\gamma^-(\zeta_{n,j})\right)^2\right)\gamma^-(\zeta_{n,j})\right]\\ (E_{nj0}^+;E_0^-)=\left[\gamma^+(\zeta_{n,j});\dfrac{1}{\phi_{n,j}^2}\left(\zeta_{n,j}^2+\left(1-\dfrac{3}{4}\gamma^+(\zeta_{n,j})\right)^2\right)\gamma^+(\zeta_{n,j})\right]\end{cases} \tag{14}$$

Depending on the initial E_0, the system will behave differently. Nguyen [17] demonstrated that the most efficient case that leads quickly to a stable and an efficient TET is when $E_0>E_0^+$. In this case the main system crosses the bifurcation and is quickly attracted to the low branch of the curve, which leads to a jump down for the energy of the main system. This jump demonstrates an efficient TET from the main linear system to considered attachments, and reduces significantly vibrations of the master structure. This criterion will be endowed to design an efficient NES. As soon as we know the initial condition of the system, i.e., an estimation of the energy E_0 to be controlled, we will be able to evalu-

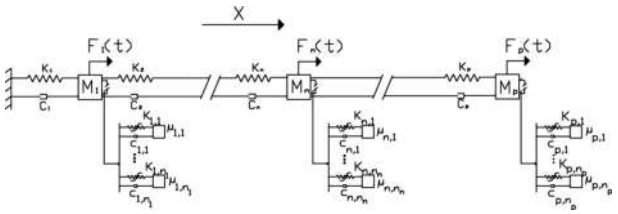

Fig. 1 The general view of the system under consideration

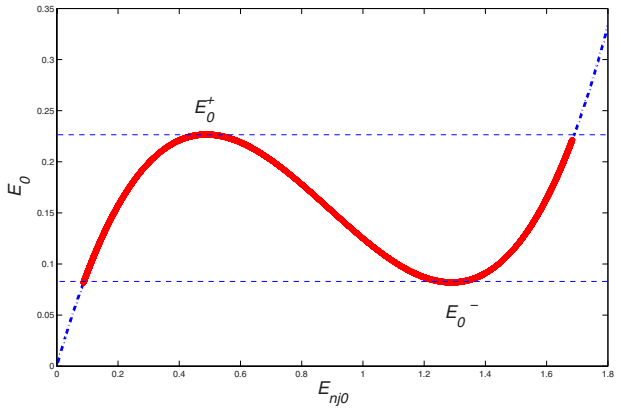

Fig. 2 Multiplicity of solution between dimensionless variables E_0 and E_{nj0}, with ζ_{nj}=0.25 and ϕ_{nj}=1

ate physical parameters of the NES that will immediately trigger the energy pumping and will establish an efficient control. The optimal case for E_0 is to be just above E_0^+; otherwise, if E_0 is too high, the system will take time to dissipate the energy before reaching the threshold of the TET. A convenient design for the NES is

$$\begin{cases} E_0 \in [E_0^+, E_0^+ + \chi] \\ E_0^+ = \dfrac{1}{\phi_{n,j}^2}\left(\zeta_{n,j}^2 + \left(1 - \dfrac{3}{4}\gamma^-(\zeta_{n,j})\right)^2\right)\gamma^-(\zeta_{n,j}) \\ \Rightarrow \Omega_{n,j}|\varphi_{00}|^2 \in [E_0^+; E_0^+ + \chi] \end{cases} \tag{15}$$

where χ is a fraction of E_0^+. We finally obtain the tuning for the stiffness of the NES j, which is attached to the DOF n of the modal shape $\phi_{n,j}$ as follows:

$$\begin{cases} k_{n,j} \in [k_{\text{opt}}, k_{\text{opt}} + \chi] \\ k_{\text{opt}} \approx \dfrac{\mu_{n,j}\omega_0^{*4}}{\phi_{n,j}^2|\varphi_{00}|^2}\left(\zeta_{n,j}^2 + \left(1 - \dfrac{3}{4}\gamma^-(\zeta_{n,j})\right)^2\right)\gamma^-(\zeta_{n,j}) \end{cases} \tag{16}$$

The main results of this analytical study presented in Eqs. (9), (10), and (16) underline the interest of using parallel NESs instead of a single NES. Let us consider a NES with the mass m, damping c, and nonlinear stiffness k_{nl}. This NES can be easily replaced with two identical parallel NESs with masses $m/2$ and damping c; according to Eq. (16), to keep the same level of activation, these two NESs will only require a nonlinear stiffness of $k_{\text{nl}}/2$. We notice that the use of parallel NESs allows disseminating the mass along the structure and significantly reduces the required nonlinear stiffness for activation, which could be very interesting for practical applications. Moreover, according to Eq. (9), the two NESs in parallel will have an equivalent damping of $2c$, which means that this configuration will be more efficient than the corresponding single NES system. (The equivalent damping is $2c$, but each NES keeps a damping of c, with c below the critical damping.) Finally, according to the principle of separated activation of Eq. (10), the parallel NES configuration can also be interesting to build NESs with several levels of activation that can control several modes of a linear structure, by tuning each NES or groups of NES on a chosen linear mode.

3 The System Under Harmonic Forcing

In this section the study of Sec. 2 is extended to the forced system. We investigate the periodic solution of the system in the vicinity of 1:1 resonance. Approximations of the system response, stability, and bifurcations are analytically investigated; and a tuning criterion is obtained. Then an application with two parallel NESs is studied analytically and numerically for experimental considerations. Let us consider the system of Eq. (1), where the linear system is under a harmonic excitation. Let us suppose that

$$\sum_{l=1}^{p} \phi_{l,1}\frac{F_l(t)}{M_1^*} = \varepsilon\omega_0^* F\cos(\omega t) \tag{17}$$

The analysis of harmonic solutions of the system is performed using complexification methods in the vicinity of 1:1 resonance with the external forcing $\varepsilon\omega_0^* F\cos(\omega t)$. We introduce global and internal displacements as follows:

$$\begin{cases} u(t) = q_1(t) \\ v_{n,j} = x_{n,j} - \phi_{n,1}q_1, \quad \forall\, n = 1\cdots p, \quad \forall\, j = 1\cdots n_n \end{cases} \tag{18}$$

Then Eq. (1) reads as

$$\begin{cases} (\ddot{u} + \omega_0^{*2}u) + \varepsilon\lambda^*\dot{u} + \varepsilon\displaystyle\sum_{l=1}^{p}\sum_{j=1}^{n_l}\alpha_{l,j}\phi_{l,j}\ddot{v}_{l,j} + \varepsilon\sum_{l=1}^{p}\sum_{j=1}^{n_l}\alpha_{l,j}\phi_{l,j}^2\ddot{u}_{l,j} = \varepsilon\omega_0^* F\cos\omega t \\ (\ddot{v}_{n,j} + \omega_0^{*2}v_{n,j}) + \phi_{n,j}(\ddot{u} + \omega_0^{*2}u) + \lambda_{n,j}\dot{v}_{n,j} + \Omega_{n,j}\omega_0^{*4}v_{n,j}^3 - \omega_0^{*2}v_{n,j} - \phi_{n,j}\omega_0^{*2}u = 0, \quad \forall\, n = 1\cdots p, \quad \forall\, j = 1\cdots n_n \end{cases} \tag{19}$$

Manevitch's complex variables [13] are introduced to investigate periodic solutions in the vicinity of forcing pulsation ω as follows:

$$\begin{aligned} \varphi_0 e^{i\omega t} &= \dot{u} + i\omega_0^* u \\ \varphi_{nj}e^{i\omega t} &= \dot{v}_{n,j} + i\omega_0^* v_{n,j}, \quad \forall\, n = 1\cdots p, \quad \forall\, j = 1\cdots n_n \end{aligned} \tag{20}$$

so

$$\begin{cases} \ddot{u} + \omega_0^{*2}u = \dot{\varphi}_0 e^{i\omega t} + i(\omega - \omega_0^*)\varphi_0 e^{i\omega t} \\ \forall\, n = 1\cdots p, \quad \forall\, j = 1\cdots n_n \\ \ddot{v}_{n,j} + \omega_0^{*2}v_{n,j} = \dot{\varphi}_{nj}e^{i\omega t} + i(\omega - \omega_0^*)\varphi_{nj}e^{i\omega t} \end{cases} \tag{21}$$

It is possible to suggest that the evolution of modulation variables φ_0 and φ_{nj} is slow compared with the excitation due to the external force. Under this assumption the first approximation for modulation variables may be obtained by averaging the complexification of Eq. (19) with respect to this fast time scale.

We are interested in the design of the NES, so we only consider the $(n_1+n_2+\ldots+n_p)$ last equations of Eq. (19). By averaging of these equations one can reach the following system:

$$\begin{aligned} &i\frac{\phi_{n,j}\varepsilon\sigma^*}{2}\varphi_0 + i\frac{\varepsilon\sigma^*}{2}\varphi_{nj} + \frac{\zeta_{n,j}}{2}\varphi_{nj} - \frac{3i\Omega_{n,j}}{8}|\varphi_{nj}|^2\varphi_{nj} + \frac{i\phi_{n,j}}{2}\varphi_0 + \frac{i}{2}\varphi_{nj} \\ &\quad = 0, \quad \forall\, n = 1\cdots p, \forall\, j = 1\cdots n_n \end{aligned} \tag{22}$$

with $\omega/\omega_0^* = 1 + \varepsilon\sigma^*/2$. Steady-state regime of Eq. (22) is obtained by demanding

$$\begin{aligned} \dot{\varphi}_0 &= 0 \\ \dot{\varphi}_{nj} &= 0, \quad \forall\, n = 1\cdots p, \quad \forall\, j = 1\cdots n_n \end{aligned} \tag{23}$$

so

$$\begin{cases} \forall\, n = 1\cdots p, \quad \forall\, j = 1\cdots n_n \\ (1 + \varepsilon\sigma^*)\phi_{n,j}\varphi_0 = \left(i\zeta_{n,j} - \left((1 + \varepsilon\sigma^*) - \dfrac{3i\Omega_{n,j}}{4}|\varphi_{nj}|^2\right)\right)\varphi_{nj} \end{cases} \tag{24}$$

By considering the complex conjugate of Eq. (24), we obtain

$$\begin{cases} \forall\, n = 1\cdots p, \quad \forall\, j = 1\cdots n_n \\ \left[\zeta_{n,j}^2 + \left(X - \dfrac{3\Omega_{n,j}}{4}|\varphi_{nj}|^2\right)^2\right]|\varphi_{nj}|^2 = \phi_{n,j}^2 X^2|\varphi_0|^2 \end{cases} \tag{25}$$

where $X = 1 + \varepsilon\sigma^*$. By introducing dimensionless variable $Z_{nj} = \Omega_{n,j}|\varphi_{nj}|^2$, we obtain

$$\left[\zeta_{n,j}^2+\left(X-\frac{3}{4}Z_{nj}\right)^2\right]Z_{nj}=\phi_{n,j}^2X^2\Omega_{n,j}|\varphi_0|^2 \qquad \forall\, n=1\cdots p,\quad \forall\, j=1\cdots n_n \tag{26}$$

We denote that the principle of separated activity is also verified, in the forced case, which permits using the same design method as described in Sec. 2.1. It provides

$$\frac{d\Omega_{n,j}|\varphi_{nj}|^2}{dZ_{n,j}}=\frac{1}{X^2\phi_{n,j}^2}\left[\frac{27}{16}Z_{n,j}^2-3Z_{n,j}+(X^2+\zeta_{n,j}^2)\right] \tag{27}$$

$$\begin{cases}\Delta_F(\zeta)=9X^2-\dfrac{27}{4}(X^2+\zeta^2)\\ \gamma_F^-(\zeta)=\dfrac{24X-8\sqrt{\Delta_F(\zeta)}}{27}\end{cases} \tag{28}$$

Then the tuning stiffness for each NES reads as

$$\begin{cases}\forall\, n=1\cdots p,\quad \forall\, j=1\cdots n_n\\ k_{n,j}^{\text{opt}}=\dfrac{\mu_{n,j}\omega_0^{*4}}{\phi_{n,j}^2(1+\varepsilon\sigma^*)^2|\varphi_0|^2}\left(\left[(1+\varepsilon\sigma^*)-\frac{3}{4}\gamma_F^-(\zeta_{n,j})\right]^2+\zeta_{n,j}^2\right)\gamma_F^-(\zeta_{n,j})\end{cases} \tag{29}$$

In the forced case the main point aims at finding a reasonable value for $|\varphi_0|^2$. Contrary to the impulse load case where initial conditions are known, the steady-state response of the system is unknown. The steady-state amplitude of the master system $|\varphi_0|$ seems to depend on variables φ_{nj} and can be obtained by solving Eqs. (22) and (24), which are not interesting for the design. But if we consider the behavior of a system with the TET, and, in particular, the energy exchange, it seems that the main system behaves linearly until its energy reaches the energy pumping threshold, and starts to be controlled. We can assume that the steady-state can be obtained by considering that the system behaves linearly until the energy pumping threshold is reached. Under this assumption we will tune the NES under harmonic forcing by considering

$$|\varphi_0|^2\approx(\dot u^2+\omega_0^{*2}u^2)_{\text{statio}}\approx\omega_0^{*2}u_{\text{statio}}^2\approx\frac{\varepsilon^2\omega_0^{*2}F^2}{(\omega_0^*-\tilde\omega)^2+\tilde\omega^2\varepsilon\lambda^*} \tag{30}$$

where $\tilde\omega$ is the cut pulsation; i.e., the pulsation that triggers the TET and u_{statio} (the stationary value for displacement $u(t)$) is at pulsation $\tilde\omega$.

3.1 A Special Case: The System Under Harmonic Forcing With Two NESs in Parallel. Let us suppose the linear system is coupled with two parallel NESs at the DOF n with the mode shapes $\phi_{n,1}$ and $\phi_{n,2}$. Mass, damping, and stiffness of each NES are $(\mu_{n,1},\mu_{n,2})$, $(c_{n,1},c_{n,2})$, and $(k_{n,1},k_{n,2})$, respectively. In this case Eq. (19) can be rewritten as

$$\begin{cases}(\ddot u+\omega_0^{*2}u)+\varepsilon\lambda^*\dot u+\varepsilon\alpha_{n,1}\phi_{n,1}\ddot v_{n,1}+\varepsilon\alpha_{n,2}\phi_{n,2}\ddot v_{n,2}+\varepsilon Y_2\ddot u=\varepsilon\omega_0^*F\cos\omega t\\ (\ddot v_{n,1}+\omega_0^{*2}v_{n,1})+\phi_{n,1}(\ddot u+\omega_0^{*2}u)+\lambda_{n,1}\dot v_{n,1}+\Omega_{n,1}\omega_0^{*4}v_{n,1}^3-\omega_0^{*2}v_{n,1}-\phi_{n,1}\omega_0^{*2}u=0\\ (\ddot v_{n,2}+\omega_0^{*2}v_{n,2})+\phi_{n,2}(\ddot u+\omega_0^{*2}u)+\lambda_{n,2}\dot v_{n,2}+\Omega_{n,2}\omega_0^{*4}v_{n,2}^3-\omega_0^{*2}v_{n,2}-\phi_{n,2}\omega_0^{*2}u=0\end{cases} \tag{31}$$

with $Y_2=\alpha_{n,1}\phi_{n,1}^2+\alpha_{n,2}\phi_{n,2}^2$. By introducing complex variables and averaging equations in the vicinity of 1:1 resonance with the external forcing we obtain the following system of equations:

$$\begin{cases}(1+\varepsilon Y_2)\left(\frac{1}{\omega_0^*}\dot\varphi_0+i\left(\frac{\omega}{\omega_0^*}-1\right)\varphi_0\right)+\varepsilon\alpha_{n,1}\phi_{n,1}\left(\frac{1}{\omega_0^*}\dot\varphi_{n1}+i\left(\frac{\omega}{\omega_0^*}-1\right)\varphi_{n1}\right)+\alpha_{n,2}\phi_{n2}\varepsilon\left(\frac{1}{\omega_0^{*2}}\dot\varphi_{n2}+i\left(\frac{\omega}{\omega_0^*}-1\right)\varphi_{n2}\right)+\frac{\varepsilon\zeta^*}{2}\varphi_0+\frac{i\varepsilon\phi_{n,1}}{2}\varphi_{n1}+\frac{i\alpha_{n,2}\varepsilon\phi_{n,2}}{2}\varphi_{n2}+\frac{i\varepsilon}{2}Y_2\varphi_0=\frac{\varepsilon F}{2}\\ \phi_{n,1}\left(\frac{1}{\omega_0^*}\dot\varphi_0+i\left(\frac{\omega}{\omega_0^*}-1\right)\varphi_0\right)+\left(\frac{1}{\omega_0^*}\dot\varphi_{n1}+i\left(\frac{\omega}{\omega_0^*}-1\right)\varphi_{n1}\right)+\frac{\zeta_{n,1}}{2}\varphi_{n1}-\frac{3i\Omega_{n,1}}{8}|\varphi_{n1}|^2\varphi_{n1}+\frac{i\phi_{n,1}}{2}\varphi_0+\frac{i}{2}\varphi_{n1}=0\\ \phi_{n,1}\left(\frac{1}{\omega_0^*}\dot\varphi_0+i\left(\frac{\omega}{\omega_0^*}-1\right)\varphi_0\right)+\left(\frac{1}{\omega_0^*}\dot\varphi_{n,2}+i\left(\frac{\omega}{\omega_0^*}-1\right)\varphi_{n2}\right)+\frac{\zeta_{n,2}}{2}\varphi_2-\frac{3i\Omega_{n,2}}{8}|\varphi_{n2}|^2\varphi_{n2}+\frac{i\phi_{n,2}}{2}\varphi_0+\frac{i}{2}\varphi_{n2}=0\end{cases} \tag{32}$$

We investigate the stationary response regime by requiring

$$\dot\varphi_0=\dot\varphi_{n1}=\dot\varphi_{n2}=0 \tag{33}$$

which yield to the following system:

$$\begin{cases}(1+\varepsilon Y_2)i\sigma^*\varphi_0+\varepsilon\alpha_{n,1}\phi_{n,1}i\sigma^*\varphi_{n1}+\alpha_{n,2}\phi_{n,2}\varepsilon i\sigma^*\varphi_{n2}+\zeta^*\varphi_0+i\alpha_{n,1}\phi_{n,1}\varphi_{n1}+i\alpha_{n,2}\phi_{n,2}\varphi_{n2}+iY_2\varphi_0=F\\ i\dfrac{\phi_{n,1}\varepsilon\sigma^*}{2}\varphi_0+i\dfrac{\varepsilon\sigma^*}{2}\varphi_{n1}+\dfrac{\zeta_{n,1}}{2}\varphi_{n1}-\dfrac{3i\Omega_{n,1}}{8}|\varphi_{n1}|^2\varphi_{n1}+\dfrac{i\phi_{n,1}}{2}\varphi_0+\dfrac{i}{2}\varphi_{n1}=0\\ i\dfrac{\phi_{n,2}\varepsilon\sigma^*}{2}\varphi_0+i\dfrac{\varepsilon\sigma^*}{2}\varphi_{n2}+\dfrac{\zeta_{n,2}}{2}\varphi_{n2}-\dfrac{3i\Omega_{n,2}}{8}|\varphi_{n2}|^2\varphi_{n2}+\dfrac{i\phi_{n,2}}{2}\varphi_0+\dfrac{i}{2}\varphi_{n2}=0\end{cases} \tag{34}$$

By introducing $Z_{n10}=\Omega_{n,1}|\varphi_0|^2$, $Z_{n20}=\Omega_{n,2}|\varphi_0|^2$, $Z_{n22}=\Omega_{n,2}|\varphi_{n22}|^2$, and $Z_{n11}=\Omega_{n,1}|\varphi_{n1}|^2$ and using polar form and calculating modulus, one can find the following dimensionless equations:

$$\begin{cases}\left[\left[(1+\varepsilon\sigma^*)-\frac{3}{4}Z_{n11}\right]^2+\zeta_{n,1}^2\right]Z_{n11}=\phi_{n,1}^2(1+\varepsilon\sigma^*)^2Z_{n10}\\ \left[\left[(1+\varepsilon\sigma^*)-\frac{3}{4}Z_{n22}\right]^2+\zeta_{n,2}^2\right]Z_{n22}=\phi_{n,2}^2(1+\varepsilon\sigma^*)^2Z_{n20}\end{cases} \tag{35}$$

Let us consider the case of two parallel NESs, which are attached at the same DOF, with the same damping ($\phi_{n,1}=\phi_{n,2}=\phi_n$ and $\zeta_{n,1}=\zeta_{n,2}=\zeta_n$). This case is considered intestinally for the experimental studies that will be presented later; nevertheless, the following analytical study could be undertaken for $\phi_{n,1}\neq\phi_{n,2}$ with similar method. The two NESs are tuned on the same level of activation as follows:

$$\frac{k_{n,1}}{\mu_{n,1}}=\frac{k_{n,2}}{\mu_{n,2}}\Rightarrow\Omega_{n,1}=\Omega_{n,2}=\Omega_n \tag{36}$$

Then we obtain algebraic relations between Z_{n11} and Z_{n22} as follows:

$$Z_{n11}=Z_{n22} \tag{37}$$

$$Z_{n11}=-\frac{1}{2}Z_{n22}+\frac{4X}{3}\pm\frac{1}{6}\sqrt{48XZ_{n22}-27Z_{n22}^2-64\zeta_n^2} \tag{38}$$

Equation (38) is not physically relevant as it does not verify Eq. (35). Then we have

$$|\varphi_{n1}|^2=|\varphi_{n2}|^2\Rightarrow\varphi_{n1}=\varphi_{n2}\quad\text{(see Eq. (34))} \tag{39}$$

and the following reduced system:

$$\begin{cases}(i[XY+\sigma^*]+\zeta^*)\varphi_0+\frac{i}{\phi_n}XY\varphi_{n1}=F\\ iX\phi_n\varphi_0+iX\varphi_{n1}-\frac{3i\Omega_n}{4}|\varphi_{n1}|^2\varphi_{n1}+\zeta_n\varphi_{n1}=0\end{cases} \tag{40}$$

After some mathematical manipulations the behavior of the system in terms of φ_{n1} can be expressed as

$$\begin{cases}\frac{i\phi_nXF(\zeta_n-i[XY+\sigma^*])}{K}=\left[i\left(\frac{X^2Y[XY+\sigma^*]}{K}-X+\frac{3\Omega_n}{4}|\varphi_{n1}|^2\right)-\left(\frac{X^2Y}{K}\zeta^*+\zeta_n\right)\right]\varphi_{n1}\\ K=(XY+\sigma^*)^2+\zeta^{*2}\end{cases} \tag{41}$$

By evaluating the modulus, we find out that

$$\frac{\phi_n^2X^2Z_F}{K}=\left[\left(\frac{X^2Y[XY+\sigma^*]}{K}-X+\frac{3}{4}Z_n\right)^2+\left(\frac{X^2Y}{K}\zeta^*+\zeta_n\right)^2\right]Z_n$$
$$\text{with}\quad Z_F=\Omega_n|\varphi_0|^2\quad\text{and}\quad Z_n=\Omega_n|\varphi_{n1}|^2 \tag{42}$$

Equation (42) is polynomial of order 3 in terms of Z_n. It can be written under the following general form:

$$\begin{cases}p_3Z_n^3+p_2Z_n^2+p_1Z_n+p_0=0\\ \text{with}\\ p_3=\frac{9}{16}\\ p_2=-\frac{3X}{2}+(\sigma^*+XY)\frac{3X^2Y}{2K}\\ p_1=(X^2+\zeta^{*2})+\frac{2X^2Y}{K}(\zeta_n\zeta^*-\sigma^*+X-X^2Y)+\frac{X^4Y^2}{K^2}(\zeta^{*2}+(\sigma^*+XY)^2)\\ p_0=-\frac{\phi_n^2X^2Z_F}{K}\end{cases} \tag{43}$$

The roots of this polynomial are the values of Z_n at each step of frequency. The behavior of the main system can be expressed by the following system:

$$Z_F=\frac{1}{\phi_n^2(1+\varepsilon\sigma^*)^2}\left[\left[(1+\varepsilon\sigma^*)-\frac{3}{4}Z_n\right]^2+\zeta_n^2\right]Z_n$$
$$u_{\text{statio}}^2\approx\frac{Z_F}{\omega_0^*\Omega_n} \tag{44}$$

3.2 Multiple Solutions and Linear Stability Analysis

3.2.1 Multiplicity of Periodic Solutions. The polynomial of Eq. (43) can exhibit multiple solutions. We will investigate the case of the shift between one single real solution and three real solutions. The polynomial of Eq. (43) reads as

$$p_3Z_n^3+p_2Z_n^2+p_1Z_n+p_0=0 \tag{45}$$

which can be written in the Cardan form

$$\begin{cases} T^3 + pT + q = 0 \\ \text{with} \\ p = \dfrac{p_1}{p_3} - \dfrac{p_2^2}{3p_3^2} \\ q = \dfrac{p_2}{27p_3}\left(\dfrac{2p_2^2}{p_3} - \dfrac{9p_1}{p_3}\right) + \dfrac{p_0}{p_3} \end{cases} \tag{46}$$

According to the Cardan formulas the double roots $\bar{T}$ can be expressed as

$$\bar{T} = \frac{-3q}{2p} \Rightarrow \bar{Z}_n = \frac{p_1p_2 - 9p_3p_0}{6p_1p_3 - 2p_2^2} \tag{47}$$

As a double root $\bar{Z}_n$ is also solution of the first derivative of Eq. (45) as

$$3p_3\bar{Z}_n^2 + 2p_2\bar{Z}_n + p_1 = 0 \tag{48}$$

Combination of Eqs. (47) and (48) gives the following equation for the border between single periodic solution and three periodic solutions:

$$3p_3(p_1p_2 - 9p_3p_0)^2 + 2p_2(p_1p_2 - 9p_3p_0)(6p_1p_3 - 2p_2^2) + p_1(6p_1p_3 - 2p_2^2)^2 = 0 \tag{49}$$

3.2.2 Linear Stability Analysis. To prevent the system from unpredicted behaviors, the stability of fixed points of Eq. (32), i.e., solutions of polynomial of Eq. (43), must be investigated. By introducing Eq. (39) in Eq. (32) the following system is obtained:

$$\begin{cases} (1+\varepsilon Y_2)\left(\dfrac{1}{\omega_0^*}\dot{\varphi}_0 + \dfrac{i\varepsilon\sigma^*}{2}\varphi_0\right) + \dfrac{\varepsilon Y}{\phi_n}\left(\dfrac{1}{\omega_0^*}\dot{\varphi}_{n1} + \dfrac{i\varepsilon\sigma^*}{2}\varphi_{n1}\right) + \varepsilon\left(\dfrac{\zeta^*}{2} + iY\right)\varphi_0 + \dfrac{i\varepsilon Y_2}{2\phi_n}\varphi_{n1} = 0 \\ \phi_n\left(\dfrac{1}{\omega_0^*}\dot{\varphi}_0 + \dfrac{i\varepsilon\sigma^*}{2}\varphi_0\right) + \left(\dfrac{1}{\omega_0^*}\dot{\varphi}_{n1} + \dfrac{i\varepsilon\sigma^*}{2}\varphi_{n1}\right) + \dfrac{\zeta_n}{2}\varphi_{n1} - \dfrac{3i\Omega_n}{8}|\varphi_{n1}|^2\varphi_{n1} + \dfrac{i\phi_n}{2}\varphi_0 + \dfrac{i}{2}\varphi_{n1} = 0 \end{cases} \tag{50}$$

We first linearize Eq. (32) in the vicinity of the steady-state response to investigate the stability of fixed points. Let us introduce small perturbations to the fixed points as follows:

$$\begin{cases} \varphi_0 = \varphi_{00} + \chi_0, & |\chi_0| \ll |\varphi_{00}| \\ \varphi_{n1} = \varphi_{n10} + \chi_{n1}, & |\chi_{n1}| \ll |\varphi_{n10}| \end{cases} \tag{51}$$

By progressing until second order expansions, the system of linearized equations can be expressed as

$$\begin{cases} (1+\varepsilon Y_2)\left(\dfrac{1}{\omega_0^*}\dot{\chi}_0 + \dfrac{i\varepsilon\sigma^*}{2}\chi_0\right) + \dfrac{\varepsilon Y_2}{\phi_n}\left(\dfrac{1}{\omega_0^*}\dot{\chi}_{n1} + \dfrac{i\varepsilon\sigma^*}{2}\chi_{n1}\right) + \varepsilon\left(\dfrac{\zeta^*}{2} + iY\right)\chi_0 + \dfrac{i\varepsilon Y_2}{2\phi_n}\chi_{n1} = 0 \\ \phi_n\left(\dfrac{1}{\omega_0^*}\dot{\chi}_0 + \dfrac{i\varepsilon\sigma^*}{2}\chi_0\right) + \left(\dfrac{1}{\omega_0^*}\dot{\chi}_{n1} + \dfrac{i\varepsilon\sigma^*}{2}\chi_{n1}\right) + \dfrac{\zeta_n}{2}\chi_{n1} - \dfrac{3i\Omega_n}{8}\varphi_{n10}^2\bar{\chi}_{n1} - \dfrac{3i\Omega_n}{4}|\varphi_{n10}|^2\chi_{n1} + \dfrac{i\phi_n}{2}\chi_0 + \dfrac{i}{2}\chi_{n1} = 0 \end{cases} \tag{52}$$

Equation (50) is a linear system that can be written in a matrix form as

$$\begin{pmatrix} \dot{\chi}_0 \\ \dot{\chi}_{n1} \\ \dot{\bar{\chi}}_0 \\ \dot{\bar{\chi}}_{n1} \end{pmatrix} = A \begin{pmatrix} \chi_0 \\ \chi_{n1} \\ \bar{\chi}_0 \\ \bar{\chi}_{n1} \end{pmatrix} \tag{53}$$

where

$$A = \omega_0^* \begin{pmatrix} a_{11} & a_{12} & 0 & a_{14} \\ a_{21} & a_{22} & 0 & a_{24} \\ 0 & \bar{a}_{14} & \bar{a}_{11} & \bar{a}_{12} \\ 0 & \bar{a}_{24} & \bar{a}_{21} & \bar{a}_{22} \end{pmatrix} \tag{54}$$

and

$$\begin{aligned} a_{11} &= -\frac{\varepsilon}{2}(i(\sigma + Y) + \zeta_0) \\ a_{12} &= \left[\frac{\varepsilon Y(2\zeta_a - 3i\Omega_a|\varphi_{n10}|^2)}{4\phi_a}\right] \\ a_{14} &= -\frac{3i\Omega_a\varepsilon Y}{\phi_a}\varphi_{10} \\ a_{21} &= \left[-\frac{i}{2}\phi_a(1+\varepsilon Y) + \frac{\varepsilon\phi_a}{2}\zeta_0 + i\varepsilon\phi_a Y\right] \\ a_{22} &= \left[\left(-\frac{X}{2} + \frac{3i\Omega_a}{4}|\varphi_{n10}|^2 - \frac{\zeta_a}{2}\right)(1+\varepsilon Y) + \frac{\varepsilon XY}{2}\right] \\ a_{24} &= \left[\frac{3i\Omega_a}{8}(1+\varepsilon Y)\varphi_{n10}\right] \end{aligned} \tag{55}$$

Then we can evaluate the characteristic equation of the matrix A, which is a fourth order polynomial in terms of θ with coefficient depending on variable $Z_n = \Omega_n|\varphi_{n1}|^2$ as follows:

$$\begin{aligned} P(\theta) = {} & \theta^4 + [(1+\varepsilon Y)\zeta_a + \varepsilon\zeta_0]\theta^3 + g_2(Z_n^2, Z_n)\theta^2 + g_1(Z_n^2, Z_n)\theta \\ & + g_0(Z_n^2, Z_n) \end{aligned} \tag{56}$$

where $g_2(Z_n^2, Z_n)$, $g_1(Z_n^2, Z_n)$, and $g_0(Z_n^2, Z_n)$ are functions that depend on variables Z_n^2 and Z_n. By investigating the real parts of roots of polynomial function $P(\theta)$ of Eq. (56), we can establish the stability of the different solutions. A Routh–Hurwitz criterion is used to establish stable and unstable areas. To investigate the equation of the Hopf bifurcation we look for purely imaginary eigenvalues of matrix A. Let us introduce $\theta = \pm i\beta$, then Eq. (56) gives

$$\beta^4 - g_1\beta^2 + g_0 = 0 \tag{57}$$

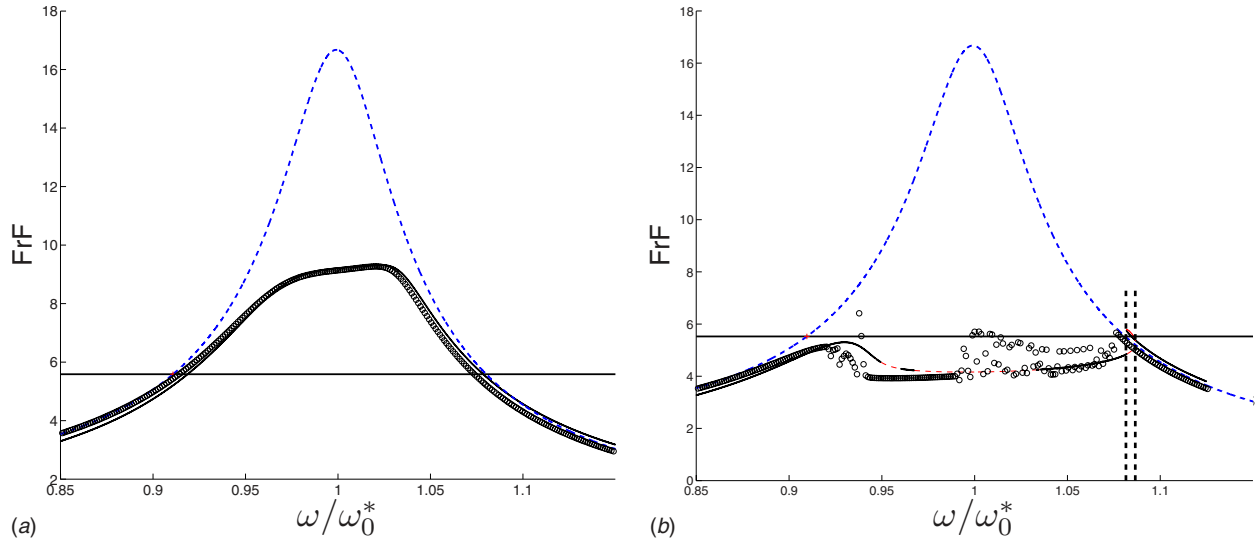

Fig. 3 FRF of the system in the vicinity of 1:1 resonance for different values of k_n. (*a*) $k_n=7\times10^4$ N m^{-3}; (*b*) $k_n=1.95\times10^5$ N m$^{-3}\approx k^{\text{opt}}$. (– – –) Analytical linear behavior, (—) analytical prediction (stable), (-.-.-.-) analytical prediction (unstable), and (∘∘∘) numerical integration.

$$-[(1+\varepsilon Y)\zeta_a+\varepsilon\zeta_0]\beta^3+g_2\beta=0 \tag{58}$$

According to Eq. (58)

$$\beta(g_2-[(1+\varepsilon Y)\zeta_a+\varepsilon\zeta_0]\beta^2)=0 \tag{59}$$

$\beta=0$ corresponds to the case $Z_F=0$, which is the unforced case and was studied previously; then we get

$$\beta=\pm\sqrt{\frac{g_2}{[(1+\varepsilon Y)\zeta_a+\varepsilon\zeta_0]}} \tag{60}$$

By introducing this result in Eq. (57) we obtain the border of the Hopf bifurcation as

$$\begin{cases} g_2^2-g_1g_2[(1+\varepsilon Y)\zeta_a+\varepsilon\zeta_0]+g_3[(1+\varepsilon Y)\zeta_a+\varepsilon\zeta_0]^2=0 \\ p_3Z_n^3+p_2Z_n^2+p_1Z_n+p_0=0 \end{cases} \tag{61}$$

3.3 Numerical Simulations. In this part numerical simulations are performed in order to compare analytical predictions of Sec. 3.1 with numerical integration of Eq. (1). These numerical simulations are performed for the case of two parallel NESs, which are attached to the same degree of freedom. System parameters are given by the following.

All initial conditions before harmonic excitation are assumed to be zero.

The amplitude of the external excitation reads as $F=0.35$ m s^{-1}.

The modal parameters of the master structure are

$$M_1^*=0.835 \text{ kg}, \quad C_1^*=M_1^*\omega_0^*\zeta^* \text{ N s m}^{-1}, \quad K_1^*=(2\pi\times4.26)^2 \text{ N m}^{-1}, \quad \varepsilon\zeta^*=3\%, \quad \phi_n=1 \tag{62}$$

The NES parameters are

$$\mu_{n,1}=\mu_{n,2}=0.03 \text{ kg}, \quad c_{n,1}=c_{n,2}=0.25 \text{ N s m}^{-1}, \quad k_{n,1}=k_{n,2}=[0.7;1.95;4]\times10^5 \text{ N m}^{-3} \tag{63}$$

The level of activation and tuning calculated from Eq. (29) is

$$\begin{cases} \text{Cut frequency: } \dfrac{\tilde{\omega}}{\omega_0^*}=\{0.9,1.08\}(\text{FRF level:}5.5) \\ \Rightarrow k_n^{\text{opt}}\approx1.95\times10^5 \text{ N m}^{-3} \end{cases} \tag{64}$$

where the cut frequency $\tilde{\omega}$ defines the intersection between the chosen activation threshold and the linear Frequency Response Function (FRF) of the system. Mode shapes have been normalized with respect to the infinite norm of mode shapes. The modal parameters represent the first mode modal parameters of a four storey prototype structure, which is used for experimental test. As we are considering the first mode and the two NESs are attached to the last storey of the structure, we have $\phi_n=1$. Since the system is under harmonic forcing, then we are interested to consider the system in the frequency domain. We study the frequency response of the system in the vicinity of 1:1 resonance for three different nonlinearity values around an optimal value. Here, the optimal value is not unique and is determined through a chosen threshold, represented by the linear behavior level of FRF at the chosen cut pulsation $\tilde{\omega}$. This threshold is investigated in Figs. 3 and 4, with cut pulsation $\tilde{\omega}/\omega_0^*=\{0.9,1.08\}$. Let us analyze the frequency response of the structure. We suppose that F is invariable and we change the nonlinearity of the NES k_n. Figures 3 and 4 represent the frequency response function in the vicinity of pulsation ω_0^* for values of k_n under (Fig. 3(*a*)), above (Figs. 4(*a*) and 4(*b*)), and near the optimal value k^{opt} (Fig. 3(*b*)). In these figures we can observe the theoretical linear behavior of the main structure in dashed line, the analytical prediction of the nonlinear behavior, which is obtained from Eq. (43), in solid line, and the numerical integration of Eq. (1) with circles. The numerical integration is computed with a MATLAB RK45 scheme; data are taken during the stationary regime, after enough periods of excitation. At each increment of frequency the initial conditions are the conditions of the previous point in the frequency sweep. This numerical sweep goes from low to high frequencies. The stability of multiple analytical solutions is highlighted: Stable periodic solutions are in solid line and unstable are plotted with dashed-dotted line. Multiple solution areas are identified by vertical dotted lines and the chosen activation threshold is plotted with a horizontal solid line. By increasing the stiffness of the nonlinear absorber, the frequency response decreases and the resonance peak breaks until the optimal design. It is obvious that the structure behaves linearly

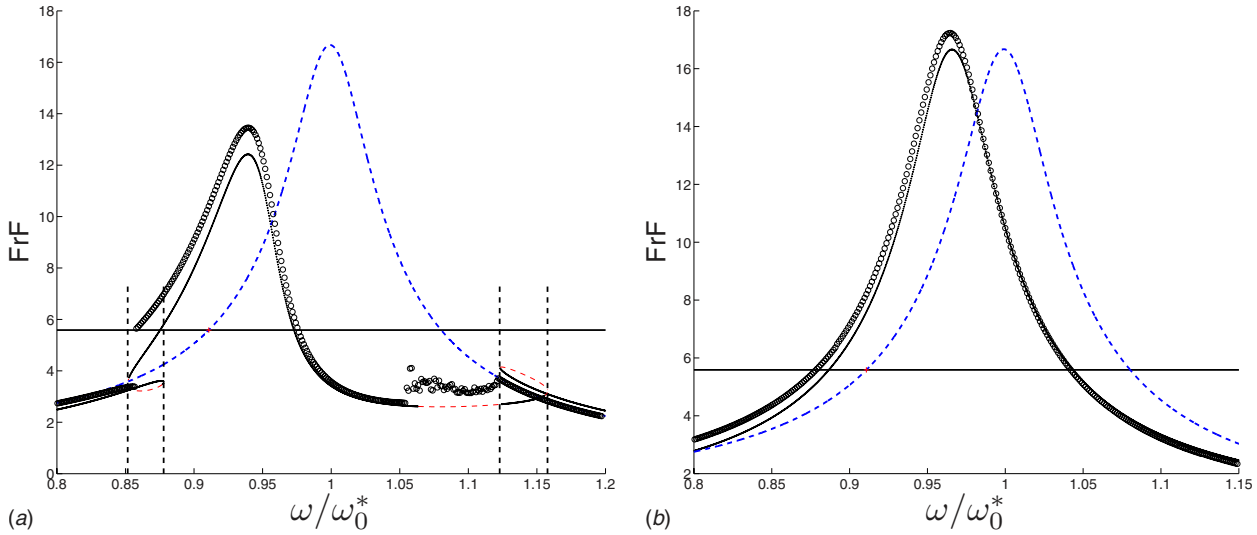

Fig. 4 FRF of the system in the vicinity of 1:1 resonance for high value of k_n. (*a*) k_n=4×10^5 $N.m^{-3}$; (*b*) $k_n \to +\infty$. (– – –) analytical linear behavior, (—) analytical prediction (stable), (-.-.-.-) analytical prediction (unstable), and (∘∘∘) numerical integration.

until it reaches the cut frequency, then strong nonlinear behavior occurs; the resonance peak is broken and the system is kept under the desired threshold, until it passes the resonance and behaves linearly again. Figure 3(*b*) illustrates the case of the optimal choice, when the NES is tuned on the chosen threshold. By increasing the nonlinear stiffness (see Fig. 4(*a*)), a new resonant peak is generated. If the nonlinear connection is increased until an infinite rigidity between the linear system and the additional absorbers masses, then this new peak turns out to the initial linear resonance peak shifted to low frequencies because of the embedded mass to the main system, as presented in Fig. 4(*b*). The occurrence of this new resonant peak reduces the efficiency of the control and can be dangerous for the system, but the occurrence of the phenomenon can be predicted by studying the multiplicity of the periodic solution of the system calculated in Eq. (49) and represented in Fig. 5. We denote also that the analytical predictions represented in Figs. 3 and 4 are in good agreement with the numerical simulations and we notice that in the unstable areas numerical results suggest that the system has no periodic solutions. The detected zones in Fig. 5 give us a good idea in choosing the right nonlinear stiffness and predicting the behavior of the system according to the chosen k_n. Here we notice that the first multiplicity of solution appears in the vicinity of $k_n \approx 1.4 \times 10^5$ N m^{-3}; above the resonance frequency, the second area of multiple solutions appears in the vicinity of $k_n \approx 1.94 \times 10^5$ N m^{-3}, which is in good agreement with the behavior of the system that is presented in Figs. 3(*b*) and 4. This argument indicates the complex and important influence of the NES on the overall behavior of the system during the TET and allows us to prevent from hazardous and uncommon behaviors.

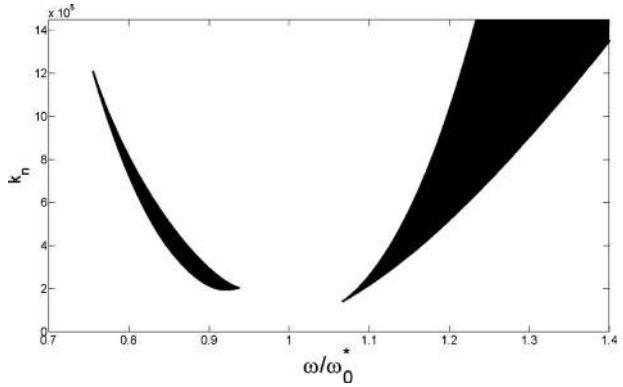

Fig. 5 Evolution of the multiplicity of periodic solutions in the plane ($\omega^*/\omega_0, k_n$)

4 Experimental Studies: A 4DOF Structure With Two Parallel NESs at the Last DOF

The test structure as shown in Fig. 6 is a four storey prototype

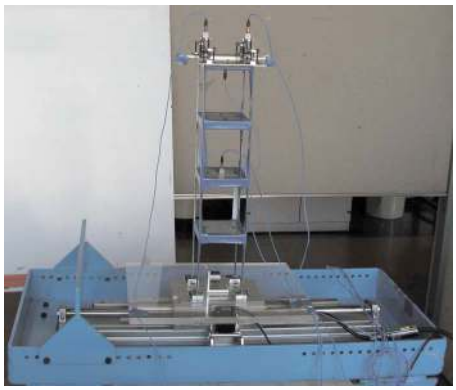

Fig. 6 The test setup and the structure

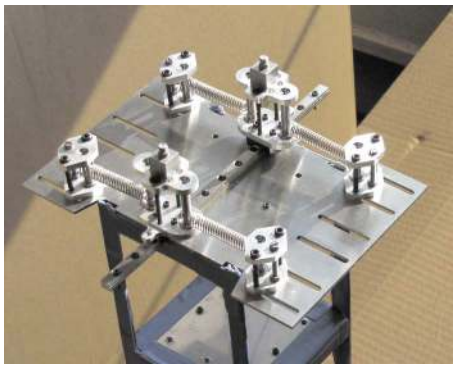

Fig. 7 Two parallel NESs at the top storey

Table 1 Main characteristics of the test structure

Mass (g)			Springs of the NES			
Main structure	NES 1	NES 2	No. of springs	l (m)	$k_{4,j}$ (N/m)	$k_{\text{nonlinear},j,4}$ (N/m^3)
2357	30	30	4	5×10^{-2}	480	1.92×10^5

steel structure. The supports of this structure are connected to a small-scale uniaxial shaking table, which is designed, built, and tested at the DGCB Laboratory of the ENTPE. The table itself is driven by a computer controlled Linmot actuator, which horizontally moves the table along linear ball bearing guide rails. The endowed acquisition system is the PAK5.4 Muller-BBM VAS, which is capable of postprocessing measured data. Two parallel NESs with a very small mass compared with the main structural mass are mounted on top of the structure, as depicted in Fig. 7. The strongly cubic nonlinear attached oscillator is composed of two mobile parts in parallel; each mobile part is anchored by two springs. Optimal stiffness values of the nonlinear springs of the NESs are obtained via the developed method, which is explained in Secs. 2 and 3. Gourdon et al. [7] illustrated that equivalent nonlinear spring for each NES system is $k_{\text{nonlinear},j,4}\approx k_{4,j}/l^2$, $j=1,2$; where l stands for the length of each linear spring of each NES. The characteristics of the system are summarized in Table 1. As illustrated in Fig. 6, five Integrated Circuit Piezoelectric (ICP) accelerometers are attached to the structure: three of them to the ground, second, and last floors; and two of them on top of mobile parts of each NES. In order to identify modal properties of the structure for feeding the nonlinear model with parallel NESs, some series of vibration tests, including shock hammer test, chirp, and sinusoidal ramp excitations, are repeated. The total mass of NESs is much smaller than the mass of the master structure, so the NES will not affect the dynamics of the master structure. In order to prevent activation of the NES system during identification process of the master system, their mobile parts are fixed. Identified frequencies and dampings of the system are reported in Table 2. The aim of this experimental studying is to transfer the energy of the first mode of the main structure to two parallel NES systems by a 1:1 resonance capture. The structure is excited by a chirp signal with sweeping frequencies between 3 Hz and 5 Hz. The absolute values of FRF of the top floor for linear case without the TET and for nonlinear case with the TET are illustrated in Fig. 8. This figure proves the capability of parallel NESs in absorbing most of the energy of the first mode. Figures 9 and 10 summarize the absolute value of the FRF of each NES during the linear and nonlinear behaviors of the structure under chirp excitations. These figures illustrate that although the main substructure endows the NES system for pumping its imposed energy, the system of NES has much less amplitudes compared with the linear case without any evidence of pumping. This means that each NES device collaborates very well with the main substructure in absorbing its energy, while during the linear state the parallel NES system becomes part of the main structure without any passive control of the induced excitation. The amplitude and phase values of parallel NESs during the pumping phenomenon are depicted in Figs. 11 and 12. Both parallel NESs move in-phase during the energy pumping phenomenon with almost equal accelerations. This behavior shows a good cooperation of parallel NESs in absorbing irreversible energy during the excitation.

Table 2 Identified frequencies and damping of the structure

	Frequency (Hz)	Damping (%)
First mode	4.44	0.41
Second mode	13.55	0.26

5 Conclusion

An analytical method for optimized design of NES devices is proposed in order to control intended modes of a linear structure

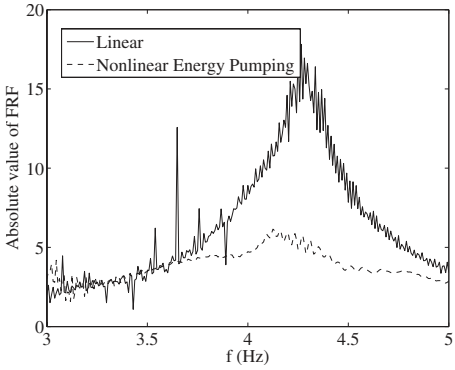

Fig. 8 The FRF of the last floor of the structure during the chirp excitation

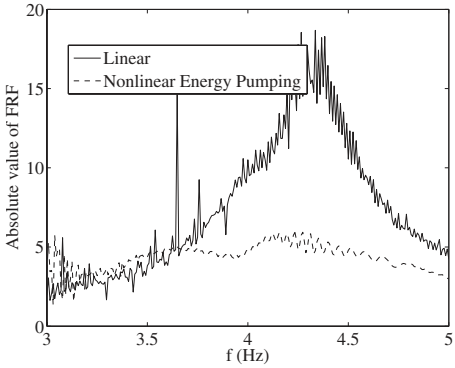

Fig. 9 The absolute values of the FRF of NES 1

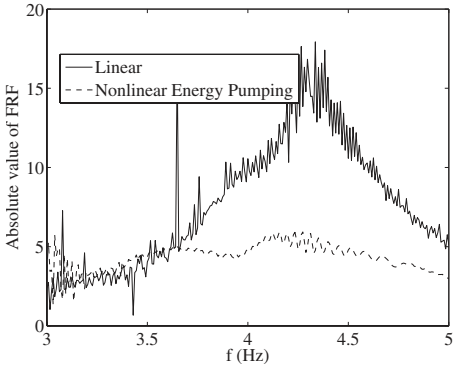

Fig. 10 The absolute values of the FRF of NES 2

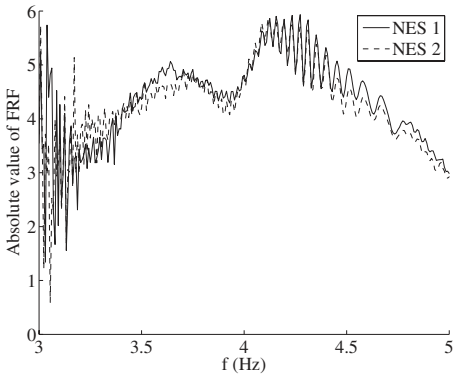

Fig. 11 The absolute values of the FRF of the NES system during the energy pumping phenomenon

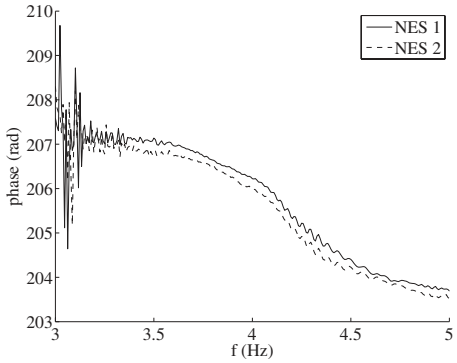

Fig. 12 The scaled phase values of the FRF of the NES system during the energy pumping phenomenon

efficiently by using the TET phenomenon. This technique is based on the study of the bifurcation, which occurs during an optimized and appropriate TET for systems under harmonic solicitations. The method leads us to comment on the efficiency of systems with parallel NESs compared with single ones; even though the effect of NES damping is not so clear in the forced case, the main conclusions are that parallel NESs offer better repartition of masses, multiple levels of activation, lower the required nonlinear stiffness, and finally result more efficient. Thanks to the developed technique, necessary parameters of the parallel NES system of a four storey prototype test structure are obtained. During seismic excitation of the structure, the nonlinear innate of two parallel NESs controlled the intended mode of the system very well. Two parallel NESs cooperated very well from the phase and amplitude points of view, and this cooperation made the main structure behave in an acceptable and controlled manner.

Acknowledgment

This work has been supported by the French National Research Agency under Contract No. ANR-07-BLAN-0193.

References

[1] Vakakis, A. F., Gendelman, O. V., Bergman, L. A., McFarland, D. M., Kerschen, G., and Lee, Y. S., 2009, *Nonlinear Targeted Energy Transfer in Mechanical and Structural Systems I*, Springer, New York.

[2] Vakakis, A. F., Gendelman, O. V., Bergman, L. A., McFarland, D. M., Kerschen, G., and Lee, Y. S., 2009, *Nonlinear Targeted Energy Transfer in Mechanical and Structural Systems II*, Springer, New York.

[3] McFarland, D. M., Bergman, L., and Vakakis, A. F., 2005, "Experimental Study of Non-Linear Energy Pumping Occurring at a Single Fast Frequency," Int. J. Non-Linear Mech., **40**(6), pp. 891–899.

[4] McFarland, D. M., Kerschen, G., Kowtko, J. J., Lee, Y. S., Bergman, L. A., and Vakakis, A. F., 2005, "Experimental Investigation of Targeted Energy Transfers in Strongly and Nonlinearly Coupled Oscillators," J. Acoust. Soc. Am., **118**(2), pp. 791–799.

[5] Kerschen, G., Kowtko, J. J., McFarland, D. M., Bergman, L. A., and Vakakis, A. F., 2006, "Theoretical and Experimental Study of Multimodal Targeted Energy Transfer in a System of Coupled Oscillators," Nonlinear Dyn., **47**, pp. 285–309.

[6] Kerschen, G., Kowtko, J. J., McFarland, D. M., Lee, Y. S., Bergman, L. A., and Vakakis, A. F., 2007, "Experimental Demonstration of Transient Resonance Capture in a System of Two Coupled Oscillators With Essential Stiffness Nonlinearity," J. Sound Vib., **299**, pp. 822–838.

[7] Gourdon, E., Alexander, N. A., Taylor, C. A., Lamarque, C.-H., and Pernot, S., 2007, "Nonlinear Energy Pumping Under Transient Forcing With Strongly Nonlinear Coupling: Theoretical and Experimental Results," J. Sound Vib., **300**(3–5), pp. 522–551.

[8] Gourdon, E., Lamarque, C.-H., and Pernot, S., 2007, "Contribution to Efficiency of Irreversible Passive Energy Pumping With a Strong Nonlinear Attachment," Nonlinear Dyn., **50**(4), pp. 793–808.

[9] Manevitch, L. I., Gourdon, E., and Lamarque, C.-H., 2007, "Towards the Design of an Optimal Energetic Sink in a Strongly Inhomogeneous Two-Degree-of- Freedom System," ASME J. Appl. Mech., **74**, pp. 1078–1086.

[10] Lee, Y. S., Kerschen, G., McFarland, D. M., Hill, W. J., Nichkawde, C., Strganac, T. W., Bergman, L. A., and Vakakis, A. F., 2007, "Suppressing Aeroelastic Instability Using Broadband Passive Targeted Energy Transfers, Part 2: Experiments," AIAA J., **45**(10), pp. 2391–2400.

[11] Lee, Y. S., Vakakis, A. F., Bergman, L. A., McFarland, D. M., Kerschen, G., Nucera, F., Tsakirtzis, S., and Panagopoulos, P. N., 2008, "Passive Non-Linear Targeted Energy Transfer and Its Applications to Vibration Absorption: A Review," Proceedings of the Institution of Mechanical Engineers, Part K: Journal of Multi-body Dynamics, **222**, pp. 77–134.

[12] Lee, Y. S., Vakakis, A. F., McFarland, D. M., and Bergman, L. A., 2010, "Non-Linear System Identification of the Dynamics of Aeroelastic Instability Suppression Based on Targeted Energy Transfers," Aeronaut. J., **114**(1152), pp. 61–82.

[13] Manevitch, L., 1999, *Complex Representation of Dynamics of Coupled Oscillators*, Kluwer, Dordrecht/Plenum, New York, pp. 269–300.

[14] Nayfeh, A., 1979, *Nonlinear Oscillations*, Wiley, New York.

[15] Gendelman, O. V., Starosvetsky, Y., and Feldman, M., 2008, "Attractors of Harmonically Forced Linear Oscillator With Attached Nonlinear Energy Sink 1: Description of Response Regimes," Nonlinear Dyn., **51**(1–2), pp. 31–46.

[16] Gendelman, O. V., 2004, "Bifurcations of Nonlinear Normal Modes of Linear Oscillator With Strongly Nonlinear Damped Attachment," Nonlinear Dyn., **37**(2), pp. 115–128.

[17] Nguyen, T. A., 2010, "Etude du comportement dynamique et optimisation d'absorbeurs non-linéaires: Théorie et expérience," Ph.D. thesis, Université de Lyon, Lyon, France.